2025 IEEE International Conference on Emerging Trends in Computing and Communication (ETCOM)
Mangalore, India. Nov 28-29, 2025

A Hybrid Approach for Efficient EV Charging: Honey Badger Algorithm-Optimized ANN for Harmonic Mitigation in Solar PV and Grid-Connected Systems

S. L. Sreedevi
Department of Electrical and Electronics Engineering
PERI Institute of Technology,
Chennai - 600028, India.
sreeperiit1362@gmail.com

K. S. Kavin
Department of Electrical and Electronics Engineering
Government College of Engineering,
Tirunelveli, Tamil Nadu, India
kavinksk@gmail.com

V. Gomathi
Department of Electrical and Electronics Engineering
Dhanalakshmi Srinivasan College of Engineering,
Coimbatore - 641105, India.
gomathime2013@gmail.com

Ramraj B
Department of Electrical and Electronics Engineering
Nandha Engineering College,
Erode - 638052, India.
rajuvcet@gmail.com

N. Jothippriya
Department of Electrical and Electronics Engineering
Erode Sengunthar Engineering College,
Perundurai, Erode - 638057, India.
jothippriyan@gmail.com

Debarchita Mishra
Department of Electrical and Electronics Engineering
Vels Institute of Science, Technology and Advanced Studies,
India.
debarchita.se@vistas.ac.in

***Abstract*— This manuscript presents a novel Hybrid Artificial Intelligence (AI) framework that incorporates a Unified Power Quality Conditioner (UPQC) to regulate power disturbances and improves the power quality and reliability of solar Photovoltaic (PV) and grid-connected Electric Vehicle Charging Stations (EVCS). For precise management of UPQC under dynamic and nonlinear loading conditions, the Honey Badger Algorithm (HBA)-optimized Artificial Neural Network (ANN) is the main innovation. The dual function of the UPQC is to enable stable bidirectional power flow between the load, distributed Renewable Energy Sources (RES) like solar PV arrays, and EVs using supercapacitor while simultaneously reducing power quality problems including voltage sags, swells, and current harmonics. Over thorough simulations in MATLAB/Simulink, the proposed hybrid HBA-ANN methodology is verified, and its performance is contrasted with that of traditional optimization methods. The outcomes show significant gains in energy transfer efficiency, voltage stabilization and Total Harmonic Distortion (THD) reduction of (1.56%), demonstrating the efficacy of this clever, power-quality-aware EV charging system. A future-ready solution for intelligent and robust EV charging infrastructure is ensured by the combination of adaptive neural control and intelligent optimization model.**

Keywords*— *UPQC, PV, EV charging, ANN, Honey Badger Algorithm, supercapacitor, Power quality.

I. INTRODUCTION

A fantastic drive to reduce the enormous use of greenhouse gases and fossil fuel resources arose in the automobile industry with the development of EVCS, have become the most common infrastructure, especially in cities. EVs are Distributed Energy Resources (DERs) and strategic design of power supply network and investments in DERs are greatly influenced by their accessibility. [1-2]. Maximising the advantages of EVCSs for the electricity grids and securing additional service grids from EV charging stations are the two main obstacles . Utilised as power filters in bandwidth regulation, load shifting and generation balancing, these EVCSs along with STATCOM created a three-phase solar PV system with a UPQC as part of an integrated strategy [3].

PQ issues are resolved by using Active Power Filters (APFs), which are selected due to its quicker and more potent compensatory capabilities. In general, the series converter lowers supply voltage disturbances and voltage harmonics. As demonstrated by [4-5], parallel-connected converter help to mitigate problems with reactive power loads, current distortions and current harmonics. A UPQC, which combines series and parallel APFs, reduces present and voltage-based distortions. [6-7]. The DC-UPQC technique included a superconducting magnetic energy storage (SMES) system, a parallel-side DAB, and a series-side Distribution Static Synchronous Compensator (DAB) [8]. Their investigation concentrated on resolving oscillations in DC voltage caused by asymmetrical defects on the AC side. Nevertheless, PFC capacity and reactive power adjustment are not highlighted in the study. Presented a p–q theory that focused on combining PVwith UPQC [9]. Nevertheless, the impact of voltage and current harmonics is not considered in the study.

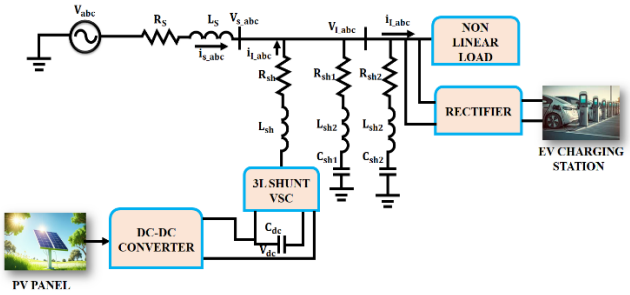

Fig. 1. General Model of UPQC with EV charging

A. Overview of AI models

Combining Particle Swarm and Grey Wolf Optimization techniques with FOPIDC designed to efficiently correct for reactive power and harmonic distortion under both balanced and unbalanced loading circumstances by controlling UPQC converter. [10]. Here, PSO-GWO technique is used to modify

the FOPID controller's parameters in order to lessen the influence of harmonics. This method seeks to adjust distribution networks for reactive power and harmonics [11]. To account for reactive power and harmonics, a filter that is economical is the Robust Extended Complex Kalman Filter approach [12]. The highest reference current values accomplished by the use of a brand-new Self-Adaptive Fuzzy-PID Controller. To solve PQ difficulties like voltage inconsistencies, lowering current signal THD, and maintaining DCLCV consistently, The FLC is deployed for series filter integrated into grid-tie three phase distribution system [13]. Nevertheless, a PIC based on the SRFT technique was specifically designed to connect to the synchronous uninterruptible active power filter linked to the fuel cell. Additionally, two scenarios with different loads demonstrated the controllers' efficiency, through the harmonics has to be reduced [14]. Henceforth, the proposed model uses a novel controller model by the aim of overcoming conventional issues related PQ.

B. Contributions

- Honey Badger Algorithm-optimized intelligent UPQC control with ANN for real-time power quality improvement.
- Mitigation of current harmonics and voltage sags/swells simultaneously in AC source connected and PV-assisted scenarios for EV charging.
- EVCS and solar energy are seamlessly integrated with the load to provide steady and dependable energy exchange.
- Enhanced system performance with regard to adaptive control, THD reduction, and power factor correction under dynamic loads.

II. Description of Proposed System

The block diagram in Fig. 2 shows a solar PV-based EVCS coupled with an advanced UPQC framework, optimised by an ANN under the direction of HBA. In addition to ensuring effective, steady operation under dynamic loading and renewable energy situations, the system is designed to improve power quality. In order to fine-tune control settings for voltage and current regulation of series and parallel converter, the ANN is trained using HBA, which simulates the foraging and digging behaviour of honey badgers, utilising real-time power quality inputs. Under nonlinear and uncertain circumstances, proposed control technique enables precise and adaptive compensation.

A solar PV panel is integrated into the lower part, for providing energy to UPQC's DC link and EVCS. A boost converter used to boost up the lower amount of energy into higher level. This setup facilitates effective energy management between AC supply, solar PV and EV while supporting bi-directional power flow from supercapacitor.

III. Proposed Methodology

A. PV model and Boost converter

The PV model and Boost Converter are essential components of the proposed UPQC-based EVCS framework for utilizing RES and guaranteeing effective power delivery. As a sustainable power source for the charging system, the PV model absorbs solar irradiance and transforms it into DC electrical energy. Nevertheless, the PV array's output voltage is intrinsically nonlinear and varies according to external factors like temperature and solar intensity. This fluctuating DC voltage is boosted by a Boost Converter for powering EVCS also UPQC's DC link. A DC-DC power electronic interface called Boost converter raises unregulated PV output voltage to a desirable, steady level that is appropriate for UPQC DC-link. It guarantees that the PV system continuously provides enough voltage to enable EV charging and the functioning of the UPQC.

B. UPQC Model

A DC-side capacitor connects UPQC, which is unified into PSC and SSC. Equations (1) and (2) are used to express the grids and SSC's active and reactive power is given as follows:

$$\begin{cases} P_{grid} = P_{grid}^{+} + P_{grid}^{-} + P_{gridm} \\ q_{grid} = 0 \end{cases} \quad (1)$$

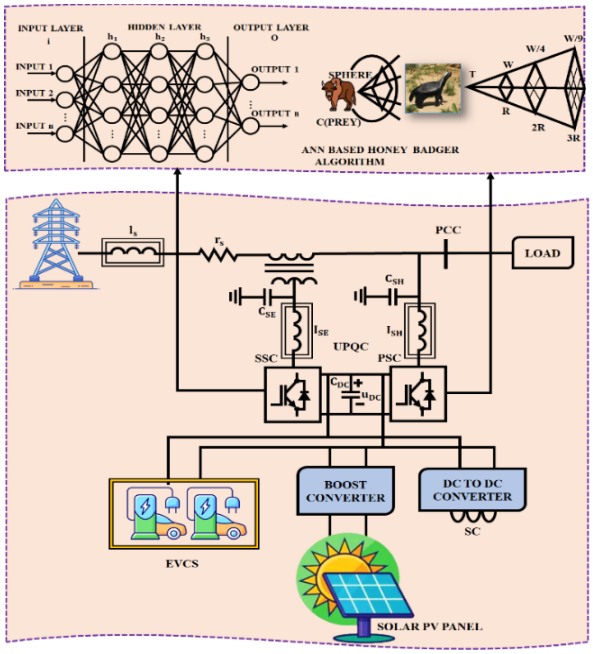

Fig. 2. UPQC with PV based EV charging

$$P_{SSC} = P_{SSC}^{+} + P_{SSC}^{-} + P_{SSCn}$$
$$q_{SSC} = 0 \quad (2)$$

The grid's total active power is represented by P_{grid}, its total reactive power by q_{grid}, total active power of SSC by P_{SSC}, q_{SSC} is represented by reactive power its fundamental positive sequence of grid power signified as P_{grid}^{+}, P_{grid}^{-} denotes negative sequence of grid power, P_{gridm} indicates harmonic power, P_{SSC}^{+} specifies positive sequence of SSC power , P_{SSC}^{-} stands for negative sequence of SSC power and P_{SSCn}states harmonic power of SSC. Power transmission over AC source and SSC is how the transformer's final power, P_{SSC}^{+} is accomplished. Equation (3) provides the following description of the reference current based on the grid voltage,

$$i_{p-REF} = \frac{2P_{SUB}}{3u_{d-grid}} \quad (3)$$

In this case, P_{SUB} stands for the DC sub-grid's power and i_{p-REF} for the power control's reference current. The active power needed to generate the switching signal is transmitted to the controller when i_{p-REF} is sent. Equations (4) and (5) are used to express the dq axis reference current as follows:

$$i_{d-REF} = i_{idav} + i_{d-REF} + i^{*} \quad (4)$$

$$i_{q-REF} = 0 \quad (5)$$

Equation (6) provides the reference load current, stated below:

$$i_c = i_{i-REF} - i_I \quad (6)$$

Equations (7) and (8) are used to characterize the grids and PSC's active with reactive power as follows:

$$\begin{cases} P_l = P_l^{+} + P_l^{-} + P_{ln} \\ q_l = 0 \end{cases} \quad (7)$$

$$\begin{cases} P_{PSC} = P_{PSC}^{+} + P_{PSC}^{-} + P_{PSCn} \\ q_{PSC} = q_l \end{cases} \quad (8)$$

Here, P_l stands for the load's net active power, q_l for load's total reactive power, psc for the PSC's total active power, qSSC for the SSC's total reactive power, $P_l^{+}$for the load's fundamental positive sequence, P_l^{-} for the load's negative sequence, P_{ln} for the load's harmonic power, P_{PSC}^{+} for the PSC's fundamental positive sequence, P_{PSC}^{-} for the PSC's negative sequence, and P_{PSCn} for the PSCs' harmonic power. Equation (9) used to depict the power transfer between the PSC and the load:

$$\begin{cases} P_{grid} = p_L \\ q_{PSC} = q_l \\ p_{PSC}^{+} = P_{SSC}^{+} \end{cases} \quad (9)$$

All active and reactive load powers are acquired via the grid and PSC.

C. ANN controller For Shunt and parallel converter

Actual currents are used as output data for training ANN shunt model by selecting hidden layers, whereas load currents $(ILa, ILb, ILc), Idc, IPV, and\ Ib$ have been used as input signals for producing reference signals. The reference current signals are produced, compared to actual currents and then sent via hysteresis controller to produce pulses that turn the IGBTs on and off as seen in Fig. 4. Figure 3 shows ANN model of the shunt and parallel compensator. The model generates three outputs.

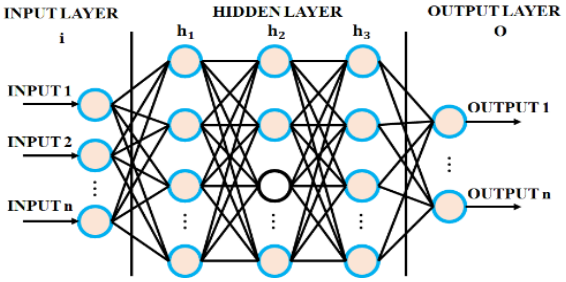

Fig. 3. Structure of ANN model for SSC and PSC control

The input layer weight is expressed as,

$$A_i = \sum_{a=1}^{n} IiE_{ij} \quad (10)$$

A_i Determines the hidden layer's activation level, H_j , while $W_{ij}$is the weight between the input and hidden layers. The activity level of the hidden layer is shown as:

$$H_j = \frac{1}{1+e^{-aj}} \quad (11)$$

The hidden layer's activity level is multiplied by output weights to forecast an output value.

$$Y_i = \sum_{j=1}^{n} H_j W_{ij} \quad (12)$$

The expected value of output produced by network is represented by (12). In order to determine the MSE, it is compared to the observed and expected output.

$$RMSE = \frac{1}{N}\sum\sqrt{[O-Y]} \quad (13)$$

In this case, N stands for sample size. Until the least RMSE is obtained, the discrepancy between the observed and anticipated outputs is reduced for each unit weight using a back-propagation learning function.

D. Honey Badger Algorithm

The Honey Badger Algorithm, a novel method presented in this paper to determine optimal value of ANN controller's gain variables. An idea is taken based on honey badgers behave in social situations. The honey badger has two strategies to find food: either it follows honey guide bird that directs it to a food supply, or it uses its senses to track and gather scent of its prey. These two situations are classified as being in digging mode and honey mode and the flowchart model is illustrated in Fig. 5 respectively. The corresponding locations of honey badgers with n populations are initialized using the following expression,

$$x_j = LB_i + r_1(UB_i - LB_i), r_1 \in [0,1] \quad (14)$$

In a group of size n, where x_j represents the honey badger's jth location and indicates a potential response, UB_i and LB_i represent the supreme and smallest limits of solution domain. The intensity is determined by the target's quantity and distance over ith and jth honey badgers (I). The target's smell potency, denoted by I_j, is as follows:

$$I_j = \frac{r_2 S}{4\pi d_j^2}, r_2 \in [0,1] \quad (15)$$

$$S = \left(x_j - x_{j+1}\right)^2 \quad (16)$$

$$d_j = x_{prey} - x_j \quad (17)$$

Where, d_j refers distance between the jth prey and badger, and S indicates equivalent to the source's intensity or centralization in density. To reduce unpredictability, the density parameter in the following equation decreased across cycles:

$$\alpha = C \times exp\left(\frac{iter}{max_{iter}}\right) \quad (18)$$

Where, C refers fixed value greater than 1 (the normal value is 2) and MaxIter denotes the highest limit of iterations.

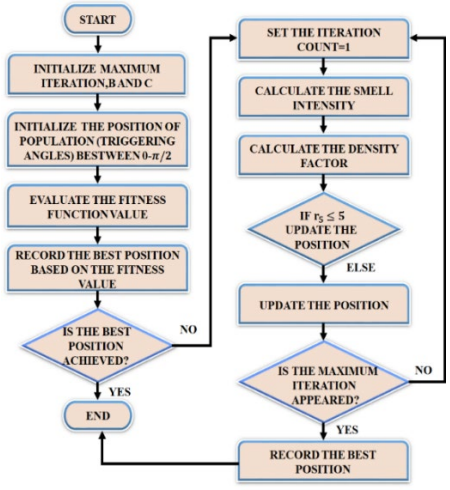

Fig. 4. Stepwise process of HBO model

Digging phase: When engaging in excavation operations, the honey badger displays a cardioid-shaped digging pattern. The approximate cardioid motion is simulated by following equation:

$$X_{new} = x_{prey} + F\beta I x_{prey} + Fr_3 a d_j |cos(2\pi r_4)[1 - cos(2\pi r_5)]| \quad (19)$$

The variable x_{prey} indicates the global optimum, or the best place to find the prey that has been caught thus far. The honey badger's ability to forage is signified as $\beta \geq 1$. the flag F modifies search approach and is chosen as below,

$$F = \begin{cases} 1 & if\ r_6 \leq 1/2 \\ -1 & otherwise \end{cases} \quad r_6 \in [0,1] \quad (20)$$

Honey phase: In the scenario when the honey badger follows the honey guide bird to find a beehive, following equation simulates the situation.

$$X_{new} = x_{prey} + a d_j r_7 F, r_7 \in [0,1] \quad (21)$$

Where, new locations of HB and its prey are denoted by X_{new} andx_{prey}, respectively. Equation (21) makes it evident that the HBA uses distance knowledge d_j to focus its search on ideal prey site (x_{prey}). Number of solutions (n), maximum number of iterations $(maxiter)$ as well as amount of state variables (d) are the three main determinants of HBA. Despite this, the additional energy from solar is stored in supercapacitor, which give supply to EV, when grid and solar unable to generate adequate supply.

IV. Results and Disucssion

The proposed control model for UPQC based EV charging is validate in this section by MATLAB/Simulink, which demonstrates unity PF, minimal harmonics and ripple as described below, the parameter specification of presented model is shown in Table I.

TABLE I. Attributes And its Value For The Proposed Model

Parameter	Specification
AC Source	
Load Resistance	100Ω
Load Inductance	$10mH$
PV system	
Open circuit voltage	$22.6V$
Short circuit voltage	$12V$

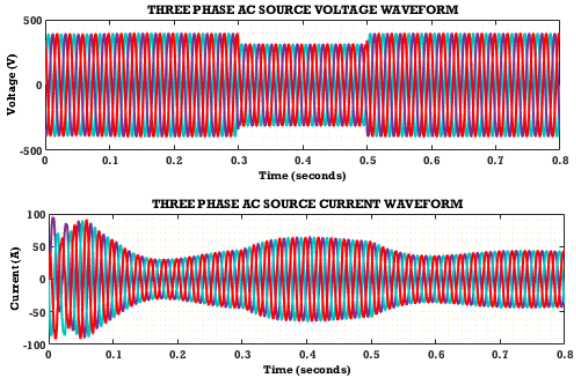

Fig. 5. Three phase AC voltage and current waveforms

Over a period of 0 to 0.8s, the voltage waveform displays a steady and balanced sinusoidal pattern with a peak amplitude of roughly 400V as signified in Fig. 5. This shows a steady supply of AC voltage free from significant deviations. By about 0.4s, the current waveform has stabilized into a sinusoidal shape after initially exhibiting distortion and harmonics.

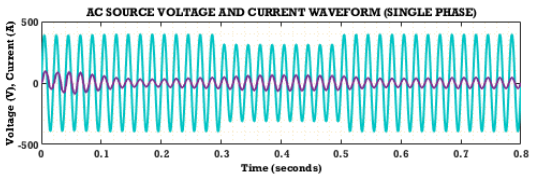

Fig. 6. AC source voltage and current waveform (zoomed single phase)

Figure 6 displays appropriate synchronization and sinusoidal behavior, overlays the voltage and current for a single phase. Following correction, the voltage and current peak readings are roughly 400V and 50A, respectively, signifies a balanced single-phase operation.

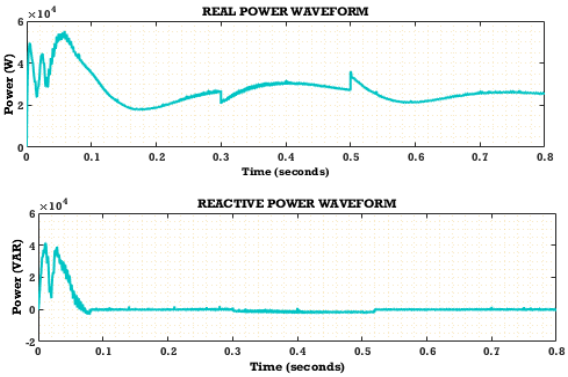

Fig. 7. Three phase real and reactive power waveform

The real power demonstrating how well the compensation works to stabilize real power. Reactive power shows large transients at first and then gradually decreasing to zero as illustrated in Fig. 7.

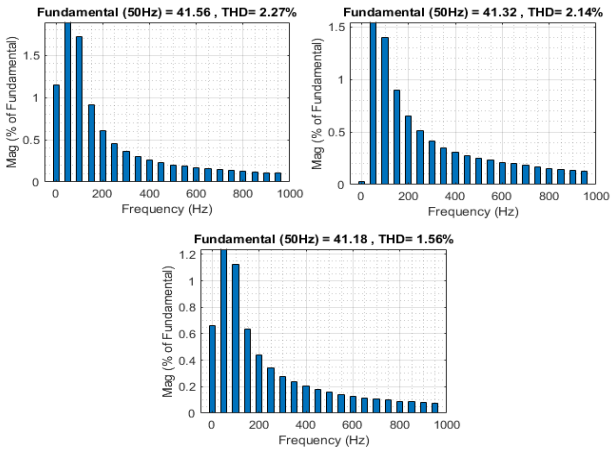

Fig. 8. THD waveforms of R, Y and B phases

The three-phase AC voltage's frequency domain analysis reveals a Total Harmonic Distortion (THD) of 2.27% for R phase, Y phase provides THD of 2.14% and B phase indicates a minimal THD of 1.56% as seen in Fig. 8.

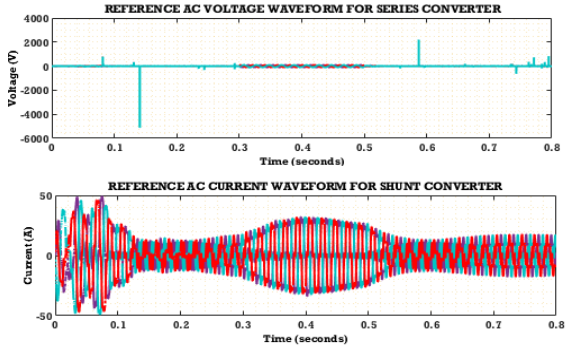

Fig. 9. Reference AC voltage and current for series and shunt converter

The series converter's reference voltage exhibits abrupt transients. Under harmonic or voltage sag/swell circumstances, these strong peaks show dynamic voltage injection for series correction. The shunt converter's reference current tracking behavior is displayed in Fig. 9. Accurate current reference generation is indicated by its first maximized transients and distorted waveforms, which eventually stabilize into a balanced sinusoidal shape.

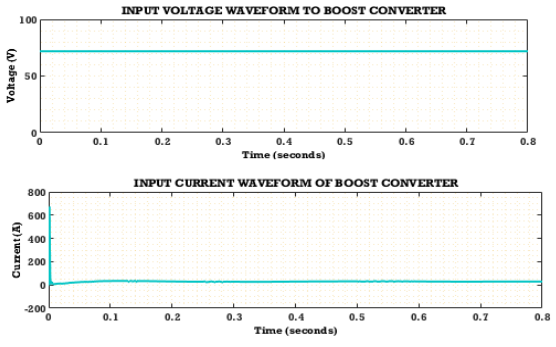

Fig. 10. Input voltage to boost converter from PV

The input voltage stays constant and ripple-free by the value of 75V when temperature and intensity maintains $25°C$ and$1000Sq/m$), demonstrating the boost converter's stable voltage input circumstances. Similarly, input current largely stays and close to 30A with no ripple as signified in Figure 10.

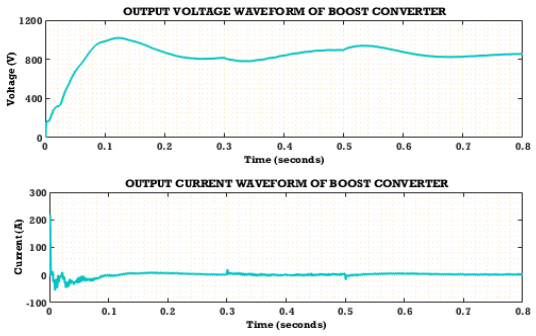

Fig. 11. Output voltage from boost converter

The boost converter's output voltage begins at about 400V and increases gradually, peaking at about 1000V in about 0.1s shown in Fig. 11. After then, for the duration of the simulation, the voltage stabilizes with little ripple. This demonstrates that the boost is operating effectively, providing a steady and controlled DC output voltage at 900V. Similarly, after 0.5s, the current waveform rapidly stabilizes at about 20A after showing a rising transient at first.

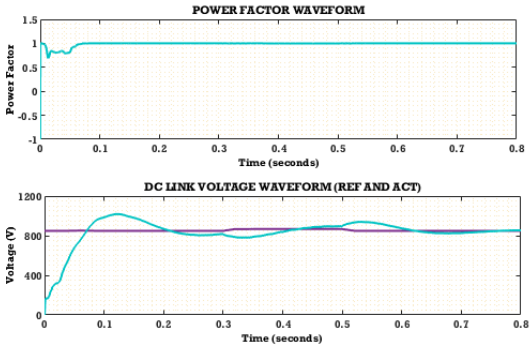

Fig. 12. PFC and DC link waveforms

With a nearly optimal power factor, the converter is operating efficiently. Both reference and actual curves reach about 900V in 0.6s, with the DC-link voltage displaying the actual voltage nearly matching the reference profile shown by Fig. 12. The robustness of the control mechanism is demonstrated precise voltage regulation necessary for DC bus stability.

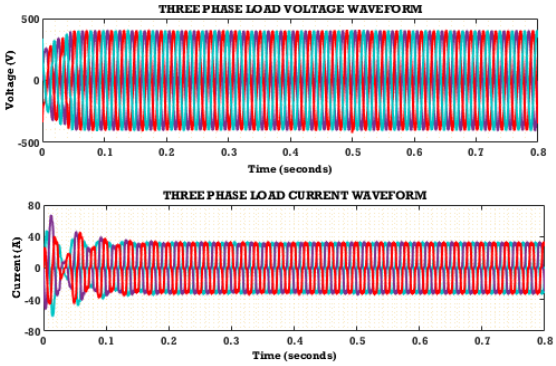

Fig. 13. Load voltage and current waveforms

The load voltage waveform in Fig. 13 shows up as a three-phase, fully sinusoidal, balanced signal with a peak of 400V. The fact that the current stabilizes after about 0.2s indicates that any disruptions or harmonics have been effectively reduced.

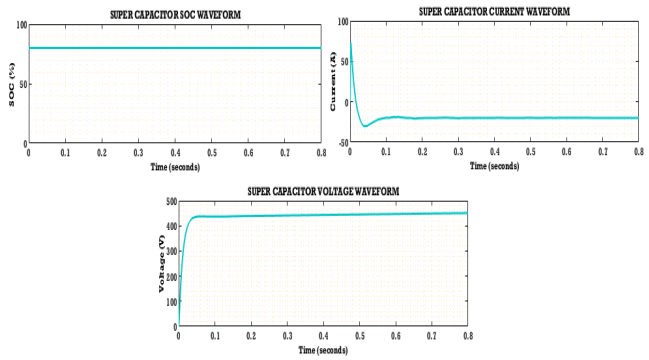

Fig. 14. Supercapacitor waveforms

During the 0.8s simulation, the SOC waveform stays constant at 90% as illustrated in Fig. 14. At the beginning of operation, Supercapacitor current waveform displays a slight peak current of roughly 80A, demonstrating the supercapacitors quick charging behavior. Within 0.1s, this current drops off rapidly and maintains around -35A. Additionally, starting at 0V, the supercapacitor voltage quickly increases to a stable operating voltage of about 420V in 0.1s.

TABLE II. CONTROLLER PERFORMANCE COMPARISON

Features	SRF Controller [15]	FUZZY Controller [13]	Proposed ANN with optimization controller)
Ripples (%)	0.15	0.5	0.12
THD	3.56	1.66	1.56

The performance comparison among different control strategies highlights the superiority of the proposed ANN with optimization-based controller. It achieves the lowest ripple percentage of 0.12% indicates in Table II. Additionally, proposed method records the lowest THD at 1.56%. These results demonstrate the enhanced power quality and dynamic performance of the proposed intelligent control strategy.

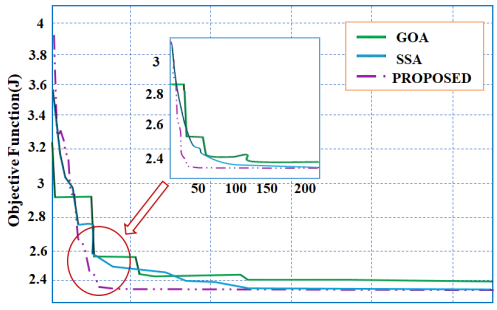

Fig. 15. Convergence curve of various optimization models

Three optimization methods are compared in the convergence graph in Fig. 15 such as GOA, proposed and SSA model. In contrast to GOA and SSA, proposed algorithm shows the fastest and most reliable convergence among them, achieving the lowest objective value.

V. CONCLUSION

The determination of this study is to expand the power quality and operational stability of solar PV and load-connected EV charging systems by implementing a unique intelligence-based control method for UPQC control. The HBA optimized ANN efficiently mitigates significant PQ problems such voltage sags, swells and current harmonics. Comparing proposed HBA-ANN methodology to traditional optimization methods. The findings show a significant decrease in THD of (1.56%) with minimal torque, enhancements in energy transfer efficiency and improvements in voltage regulation.

REFERENCES

[1] B. Shwetha, G. Suresh Babu, and G. Mallesham, “Intelligent solar PV grid connected and standalone UPQC for EV charging station load,” Results in control and optimization, vol. 15, pp. 100420, June 2024.

[2] M. SivaramKrishnan, N. Kathirvel, and T. Senjyu, “Smart charging solution for electric vehicles: Leveraging grid connected solar PV with UPQC using HBA-MORARNN approach,” Energy Reports, vol. 13, pp. 2454-2467, June 2025.

[3] K. Srilakshmi, S. Gaddameedhi, P. R. Ganesh Aravindhababu Palanivelu, and S. Selvarajan, “Optimal design of solar/wind/battery and EV fed UPQC for power quality and power flow management using enhanced most valuable player algorithm,” Frontiers in Energy Research, vol. 11, pp. 1342085, January 2024.

[4] C. S. Prasada Rao, A. Pandian, J. Massoud, and M. Shouran, “Unified power quality conditioner-based solar EV charging station using the GBDT–JS technique,” Frontiers in Energy Research, vol. 12, pp. 1343635, April 2024.

[5] S. Chapala, R. L. Narasimham, and G. R. Das, “Power Quality Analysis of ANFIS Based Distributed Generation System with UPQC,” International Journal of Engineering and Manufacturing (IJEM), vol. 14, no. 4, pp. 1-14, 2024.

[6] T. Trivedi, R. Jadeja, C. Long, P. Sanjeevikumar, and A. Ved, “Sliding mode-based direct power control of unified power quality conditioner,” Heliyon, vol. 10, no. 20, October 2024.

[7] A. R. Singh, M. Dashtdar, L. Prokop, and S. Misak, “AI-enhanced power quality management in distribution systems: implementing a dual-phase UPQC control with adaptive neural networks and optimized PI controllers,” Artificial Intelligence Review, vol. 57, no. 11, pp. 311, September 2024.

[8] B. S. Goud, C. N. S. Kalyan, G. S. Rao, C. R. Reddy, M. Shorfuzzaman, B. A. Zneid, and M. Pushkarna, “GRU controller-based UPQC compensator design for improving power quality in grid-integrated non-linear load system,” Scientific Reports, vol. 15, no. 1, pp. 19677, June 2025.

[9] Z. Reguieg, I. Bouyakoub, and F. Bouhadji, “Optimizing power quality: simulation of UPQC integrated PV with comprehensive reliability and performance analysis,” International Journal of Smart Grid, vol. 8, no. 1, pp. 47-52, 2024.

[10] K. Srilakshmi, K. Kondreddi, and R. Vangalapudi, “Grid connected and standalone renewable source fed UPQC: a hybrid control technique for power quality enhancement,” Discover Applied Sciences, vol. 7, no. 3, pp. 147, February 2025.

[11] K. Srilakshmi, G. S. Rao, K. Swarnasri, S. R. Inkollu, K. Kondreddi, and B. Khan, “Multiobjective Neuro - Fuzzy Controller Design and Selection of Filter Parameters of UPQC Using Predator Prey Firefly and Enhanced Harmony Search Optimization,” International Transactions on Electrical Energy Systems, no. 1, pp. 6611240, 2024.

[12] H. Ahmed and D. Çelik, “Enhanced UPQC control scheme for power quality improvement in wave energy driven PMSG system,” IEEE Transactions on Energy Conversion , 2024.

[13] R. Simhachalam and A. D. Goswami, “Fuzzy induced controller for optimal power quality improvement with PVA connected UPQC,” Energy Harvesting and Systems, vol. 11, no. 1, pp. 20220146, January 2024.

[14] S. Rajshekar, L. C. Saikia, and L. Nandyala, “Optimizing wind energy integration with fuzzy PID DSTACOM and hybrid MPPT for reduced harmonic distortion,” Computers and Electrical Engineering, vol. 124, pp. 110391, May 2025.

[15] H. Mahar, H. M. Munir, R. Hussain, M. F. Elnaggar, S. Kamel, and J. M. Guerrero, “Implementation of ANN controller based UPQC integrated with microgrid,” Mathematics, vol. 10, no. 12, pp. 1989, June 2022.